NANO LETTERS
Letter
pubs.acs.org/NanoLett

Atomic-Scale Observation of Multiconformational Binding and Energy Level Alignment of Ruthenium-Based Photosensitizers on TiO_2 Anatase

Christopher S. Kley,[*,†] Christian Dette,[†] Gordon Rinke,[†] Christopher E. Patrick,[‡] Jan Čechal,[†] Soon Jung Jung,[†] Markus Baur,[§] Michael Dürr,[§] Stephan Rauschenbach,[†] Feliciano Giustino,[‡] Sebastian Stepanow,[*,†,∥] and Klaus Kern[†,⊥]

[†]Max Planck Institute for Solid State Research, Heisenbergstrasse 1, 70569 Stuttgart, Germany
[‡]Department of Materials, University of Oxford, Parks Road, Oxford OX1 3PH, United Kingdom
[§]Institute of Applied Physics, Justus Liebig University Giessen, Heinrich-Buff-Ring 16, 35392 Giessen, Germany
[∥]Department of Materials, ETH Zurich, Schafmattstrasse 30, 8093 Zurich, Switzerland
[⊥]Institute de Physique de la Matière Condensée, Ecole Polytechnique Fédérale de Lausanne, 1015 Lausanne, Switzerland

Supporting Information

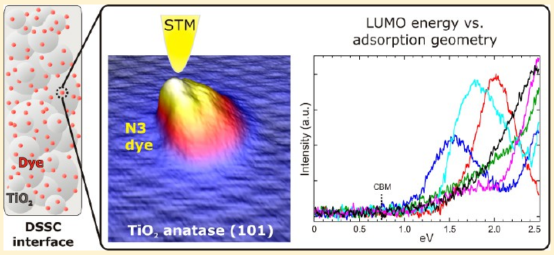

ABSTRACT: Dye-sensitized solar cells constitute a promising approach to sustainable and low-cost solar energy conversion. Their overall efficiency crucially depends on the effective coupling of the photosensitizers to the photoelectrode and the details of the dye's energy levels at the interface. Despite great efforts, the specific binding of prototypical ruthenium-based dyes to TiO_2, their potential supramolecular interaction, and the interrelation between adsorption geometry and electron injection efficiency lack experimental evidence. Here we demonstrate multiconformational adsorption and energy level alignment of single N3 dyes on TiO_2 anatase (101) revealed by scanning tunnelling microscopy and spectroscopy. The distinctly bound molecules show significant variations of their excited state levels associated with different driving forces for photoelectron injection. These findings emphasize the critical role of the interfacial coupling and suggest that further designs of dye-sensitized solar cells should target a higher selectivity in the dye-substrate binding conformations in order to ensure efficient electron injection from all photosensitizers.

KEYWORDS: *Chromophore-semiconductor interface, energy level alignment, dye-sensitized solar cells, scanning tunnelling microscopy and spectroscopy, density functional theory*

In dye-sensitized solar cells (DSSCs), ultrafast electron injection from a photoexcited dye into the conduction band of an oxide semiconductor and subsequent dye regeneration by a redox electrolyte result in photocurrent generation.[1,2] The overall performance of DSSCs strongly depends on the electron injection efficiency[3] that is linked to the electronic dye-substrate coupling[4−7] as well as the aggregation state of the photosensitizers.[8,9] Hence, a rational optimization of DSSCs would greatly benefit from the possibility of resolving and correlating photosensitizer adsorption geometries to the electronic properties of the dye-substrate interface as well as providing insights into the dye-aggregation.[9] Accordingly, apart from studying the electron injection dynamics by integral time-resolved optical spectroscopy,[10−12] much effort has been dedicated over the last decades to elucidate the structural and electronic properties of single prototypical ruthenium-based dye molecules adsorbed on oxide surfaces. In working devices, the photoelectrodes primarily consist of mesoporous nanocrystalline TiO_2 anatase films predominantly exposing the low-energy (101) surface.[13,14] Among the many photosensitizers developed for DSSCs over the past two decades, the N3 dye (cis-di(thiocyanato)-bis(2,2′-bipyridyl-4,4′-dicarboxylate)ruthenium(II))[15,16] and its derivatives[17,18] have shown consistently high performance. Previous works proposed a variety of possible N3 binding geometries and many fundamental issues, for example, the influence of the coordination geometry on the sensitizer performance, are still beyond present understanding. Studies on TiO_2 rutile immersed in N3 solution propose N3 anchoring via two carboxylic groups of the N3 biisonicotinic acid (BINA) ligands,[7,19] whereas a recent investigation on rutile substrates prepared in ultrahigh vacuum (UHV) using electrospray ion beam deposition suggests mixed-binding of the N3 molecules involving both carboxylate groups and sulfur atoms of the thiocyanate ligand.[20] Experimental data for the relevant TiO_2 anatase is scarce. Raman spectroscopy and density functional

Received: October 5, 2013
Revised: January 20, 2014
Published: January 28, 2014

dx.doi.org/10.1021/nl403717d | *Nano Lett.* 2014, 14, 563−569

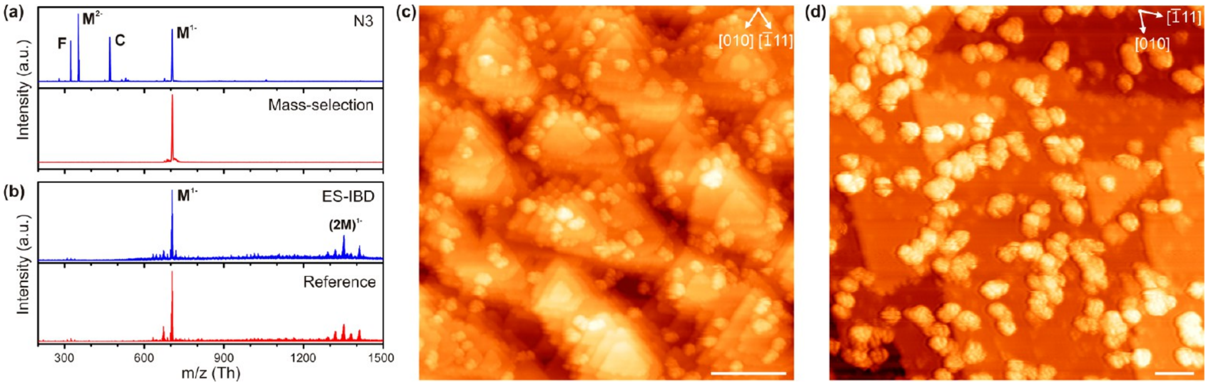

Figure 1. N3 molecules adsorbed on TiO_2 anatase (101). (a) Electrospray ionization time-of-flight mass spectra of the N3 ion beam before (top) and after (bottom) mass-selection of the singly ionized N3 molecules (F, fragment; C, cluster). (b) Negative ion mass spectra of N3 desorbed by neutral SO_2 clusters from gold surfaces onto which the dye was deposited by ES-IBD (top) and by drop-casting (bottom). (c) STM image of low N3 coverage on TiO_2 anatase (101) (deposited charge 15 pAh; 2.04 V, 0.06 nA, 5 K). (d) STM image of intermediate N3 coverage on TiO_2 anatase (101) (dep. charge 30 pAh; 1.99 V, 0.15 nA, 5 K). The crystallographic directions of the substrate were assigned according to ref 37. (Scale bar: (c) 20 nm and (d) 5 nm.)

theory (DFT) based studies indicate that the N3 molecules are bonded to the 5-fold coordinated titanium sites of the (101) surface via the carboxyl groups.[21−23] However, there is profound uncertainty about the number and mode of the carboxyl moieties binding to the substrate, that is, monodentate, bidentate bridging, and bidentate chelating.[16,24] Vibrational- and X-ray photoelectron spectroscopy indicate adsorption of the Ru-based dyes via two deprotonated carboxylate groups either in a bidentate chelating or in a bridging coordination.[25−27] According to the computational study of ref 28 the most stable model on the proton-free surface has two bidentate bridges on different BINA ligands. Instead, the calculations of ref 29 showed that three groups with monodentate linkages stabilized by surface protons represent the most stable adsorption configuration. For N719, the lowest energy configuration was found to be a bidentate/monodentate mix involving three COOH groups,[30] which was found to rearrange on anatase (101) under illumination.[31] Further, theoretical studies have cast doubt on the kinetic accessibility of the thermodynamically most-stable binding configuration of the dye molecules.[29]

Recent theoretical studies also discussed possible supramolecular interactions between the photosensitizers through hydrogen bonds and the stabilizing role of surface hydroxyl groups.[28,29,32] A further significant factor determining the device performance is the position of the lowest unoccupied molecular orbital (LUMO) of the photosensitizer with respect to the substrate Fermi level, which strongly affects the electron injection rate.[33] Thus, clarifying the question on how the dye adsorption mode influences the electronic properties is pivotal for the design of efficient sensitizers and thereby for the improvement of DSSCs. However, the direct experimental investigation of individual N3 molecules to determine the dye binding configuration and the associated electronic properties on atomically well-defined TiO_2 rutile and anatase surfaces has not been achieved so far.

Here, we investigate both the adsorption geometry and electronic characteristics of single photosensitizer N3 adsorbed on the technologically relevant TiO_2 anatase (101) substrate. In our study, atomically clean TiO_2 anatase (101) surfaces were prepared in UHV employing natural single crystals (see Methods). Electrospray ion beam deposition (ES-IBD)[34,35] was employed for gentle deposition of the thermally fragile N3 molecules onto atomically well-defined surfaces in ultrahigh vacuum at room temperature. The intactness of the deposited molecules was verified by means of soft cluster-induced desorption/ionization mass spectrometry[36] (see Methods and Supporting Information). The structural and electronic properties of the dye molecules were studied in situ by scanning tunnelling microscopy (STM) and spectroscopy (STS) at 5 K. The experimental findings are rationalized by first-principles DFT calculations.

The time-of-flight mass spectra of the N3 ion beam are presented in Figure 1a. Only single-ionized N3 molecules at 705 Th were mass-selected for deposition (bottom). Figure 1b shows mass spectra obtained by SO_2-cluster impact on gold substrates onto which N3 molecules were deposited by ES-IBD at a kinetic energy of ~5 eV (top, ES-IBD) and by drop casting (bottom, reference). They both show the same peak pattern representing the intact molecule and a dimer structure. This demonstrates that N3 fragmentation upon ion beam deposition can be excluded (for details see Supporting Information).

Figure 1c,d shows large scale STM images of N3 adsorbed on TiO_2 anatase (101). The substrate reveals characteristic trapezoidal islands with monatomic steps preferentially orientated along the [010], [11$\bar{1}$], and [$\bar{1}$11] directions.[37] The bright protrusions in the STM images have diameters of ~2.0 nm with an apparent height of ~6 Å and are assigned to single intact N3 molecules. At low N3 coverage (deposition charge 15 pAh = picoampere hour, Figure 1c), initial N3 adsorption is evidently preferred close to step edges without any preference of a particular step orientation. Only few N3 molecules adsorb isolated on terraces. As the coverage is increased (30 pAh, Figure 1d), N3 molecules assemble into larger two-dimensional clusters and chains both close to step edges and on terraces. In absence of molecular diffusion, a spatially random adsorption of N3 molecules would be expected due to the relatively strong anchoring via the carboxylic groups. The preferred N3 binding close to step edges and the formation of assemblies thus indicates transient mobility of the molecules.

Figure 2a shows a high-resolution STM image of a single N3 molecule on the atomically resolved TiO_2 anatase (101) surface. The molecule reveals an asymmetric shape where several submolecular lobes can be distinguished. The precise position of the molecular features with respect to the substrate

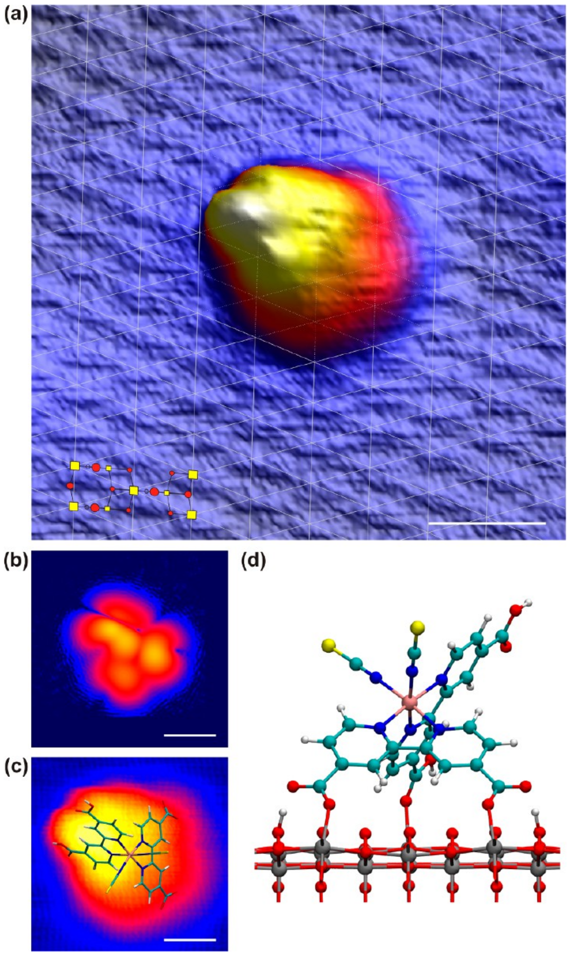

Figure 2. Photosensitizer N3 adsorbed on TiO_2 anatase (101). (a) High-resolution STM image of an individual N3 on atomically resolved substrate. The anatase (101) unit cell is indicated (red, oxygen; yellow, titanium) with the substrate lattice overlaid (each line crossing corresponds to titanium atom position); (2.0 V, 0.2 nA, 5 K). (b) Corresponding Tersoff-Hamann STM simulation. (c) N3 model overlaid to STM topograph. (d) Corresponding ball-stick N3 coordination geometry including three carboxylic groups binding to the substrate in monodentate modes. This configuration corresponds to the model "I3b" introduced in ref 29. (Scale bar: (a) 1 nm, (b) 0.7 nm, and (c) 0.7 nm; color bar for a−c see Figure 3.)

lattice can be readily determined. Comparing the experimental data to STM simulations (see below and Methods) performed for the monomers studied in ref 29 shows close agreement with a model where three carboxylic groups bind to the substrate via monodentate linkages as shown in the corresponding ball-stick model in Figure 2d. This configuration was found to be the energetically most favorable N3 adsorption mode in ref 29, owing to the minimum strain exerted on the dye molecule. However, in our experiments this adsorption configuration was observed only very rarely. In general, we observe a wealth of different N3 configurations on the surface signifying that the molecules assume a broad spectrum of possible binding modes.

Figure 3a shows a high-resolution STM image of different N3 molecules adsorbed on the TiO_2 anatase (101) surface. Each N3 molecule reveals a different shape and dissimilar submolecular features whereas the corresponding apparent heights are homogeneous (~6 Å). While the N3 molecules 1 and 4 (see Figure 3a) are characterized by broad protrusions, molecules 2 and 3 show oval shapes. These observations hint at multiple binding conformations of the N3 dyes with different adsorption energies and separating barriers, indicating that in many cases the N3 molecules are trapped in local energy minimum configurations. To analyze the experimental observations we performed DFT calculations investigating a large number of different N3 geometries by randomly varying the orientation of the N3 molecule with respect to the substrate (see Methods section for details about DFT modeling). Using the Tersoff-Hamann approximation, for each case the STM image was calculated on a plane located 2 Å above the furthest atom from the TiO_2 surface. The calculations allowed us to assign some of the observed STM motifs to specific chemical subunits of the N3 molecule. For instance, COOH groups pointing away from the substrate consistently show two prominent lobes (bottom of Figure 3b). These lobes correspond to O 2p states. Similarly the thiocyanate ligands give rise to a single spot of 1 nm diameter (middle), corresponding to S 2p states. By matching these features to our calculated STM images (Figure 3b) we were able to reconstruct the interface models displayed in Figure 3c (detailed view see Supporting Information). Note that this procedure provides an efficient and consistent approach to obtain the molecular geometries. Because of the complexity of the semiconductor−molecule−tip junction, the comparison between STM height profiles (constant current) and constant-height Tersoff-Hamann maps is not straightforward as the tip displacement amounts to 6 Å across the molecules. The N3 molecules bind in energetically much less favorable configurations such as the monodentate mode involving a hydrogen bond to the surface or the bidentate bridging mode including only one out of four N3 carboxyl groups. Further, we cannot exclude the participation of the thiocyanato ligands in the substrate bonding for other not identified N3 adsorbates. These findings demonstrate that the N3 adsorption behavior is not solely determined by the adsorption energetics but that kinetics plays a fundamental role. The access of the energetically most favorable N3 configuration appears to be kinetically hindered due to pronounced barriers originating from bond opening of anchoring carboxylic groups. The multitude of configurations observed in our study is even more surprising considering the residual ion kinetic energy of approximately 5 eV that could provide for the transient mobility after deposition giving additional impetus to overcome energy barriers.

Examining the N3 molecules 1 and 2 (Figure 3a) in more detail, the close spacing of the molecules with an elongated intermolecular protrusion indicate a dimeric supramolecular assembly. The simulated STM image and structure model are presented in Figure 3b,c (top), respectively. A plausible atomistic model of this dimer consists of two dyes anchored to the TiO_2 surface via a monodentate linkage and a bidentate bridge, respectively, with a hydrogen bond formed between two carboxylic groups facing each other. This finding is of particular importance because the electron injection efficiency is expected to be crucially influenced by the aggregation of the photosensitizers.[9] Our findings favor the recently proposed supramolecular interactions between N3 molecules based on packing considerations[28] and the reverse-engineering of core-level spectra.[29] In regard to the occurrence of various anchoring modes found for isolated dye molecules, supramolecular interactions may stabilize metastable configurations and thereby increase the number of possible adsorption geometries.

To understand the occurrence of different N3 adsorption geometries, we turn to the anchoring ligand BINA because its

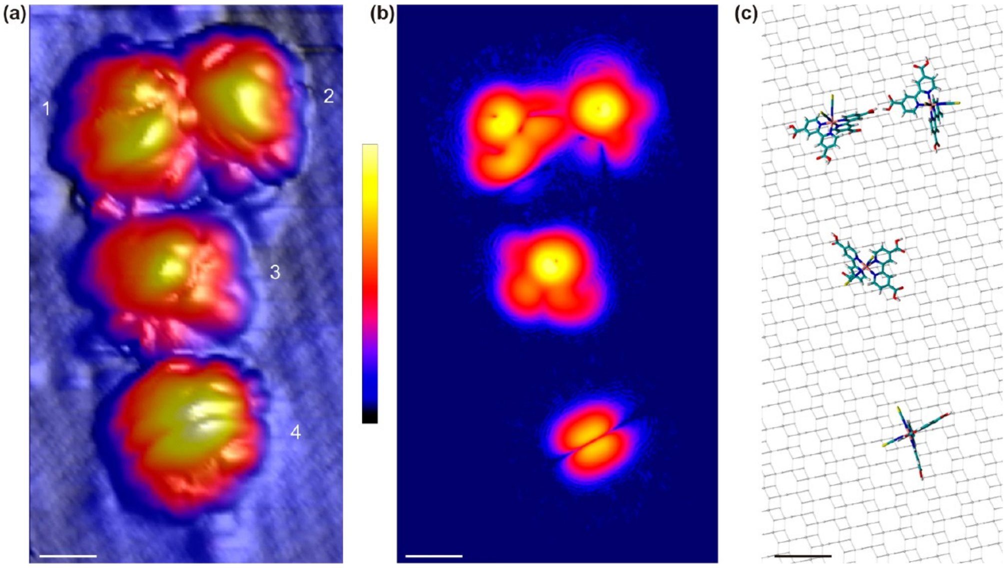

Figure 3. Individual N3 molecules on TiO_2 anatase (101). (a) High-resolution STM image revealing multiconformational N3 adsorption geometries and submolecular resolution of N3 on an atomically resolved substrate. Top two N3 molecules form a dimeric supramolecular assembly (1.72 V, 0.06 nA, 5 K). The range of the color bar is from 0 (bottom) to 6 Å (top). (b) Best matching STM simulations for the dyes in panel a. The range of the color bar is from 10^{-12} (bottom) to 10^{-5} states/Å^3 (top). (c) Corresponding ball-and-stick models of the N3 coordination geometries. (Scale bar: (a) 1 nm, (b) 1 nm, and (c) 1 nm.)

carboxylate groups are expected to dominate the N3 substrate binding and the electron transfer to the conduction band.[38−40] Figure 4a shows a high-resolution STM overview image of BINA molecules on anatase (101) deposited by thermal sublimation. Numerous different molecular adsorption geometries are revealed. One frequently observed structure is highlighted in Figure 4a and shown in greater detail in Figure 4b. This BINA configuration reveals a circular feature in the molecule center surrounded by an extended U-shaped protrusion. The binding angle amounts to ∼45° relative to the [010] direction (Figure 4b). Figure 4c,d shows the best fitting STM simulation and the corresponding adsorption model, respectively. In this particular configuration, both carboxylic groups are deprotonated with one group adsorbed in a bidentate bridge configuration and the other monodentate. A substantial twist of 40° between the pyridine rings is found[27] that is likely reduced when complexed to the N3 ruthenium. The calculated adsorption energy of this configuration is 0.88 eV and can be further stabilized in the presence of surface hydroxyls. Observing multiple BINA adsorption geometries on TiO_2 anatase (101) represents again an unexpected finding and demonstrates that also the majority of the BINA ligands cannot reach the lowest energy adsorption configuration.[41] This result suggests that the observation of multiconformational N3 adsorption can be partially attributed to a complex combination of multiple BINA coordination modes.

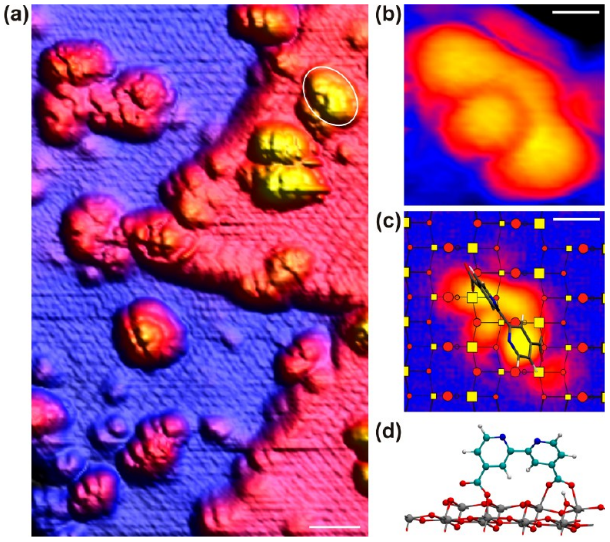

Figure 4. N3 anchoring ligand BINA adsorbed on TiO_2 anatase (101). (a) High-resolution STM overview image of BINA ligands revealing different adsorption geometries on the atomically resolved substrate (1.75 V, 0.08 nA, 5 K). (b) Magnification of a frequently observed u-shaped BINA configuration (marked in (a) by white circle). (c) Corresponding STM simulation with BINA model and substrate lattice (red, oxygen; yellow, titanium) overlaid. (d) Ball-stick model of the respective BINA adsorption geometry. (Scale bar: (a) 2 nm, (b) 0.4 nm, and (c) 0.4 nm.)

The occurrence of multiple adsorption geometries of N3 allows studying the influence of the binding on the electronic properties of the adsorbed dyes. Figure 5a shows an STM overview of N3 molecules adsorbed in different configurations and bound as monomers and dimers both on terraces and at step edges representing a realistic scenario for DSSCs (however, at a lower N3 coverage; for a full N3 monolayer see Supporting Information). Figure 5b shows STS data of the unoccupied states recorded for the individual N3 molecules marked in Figure 5a (corresponding color code). The differential conductance spectrum of the pristine TiO_2 anatase (101) surface is shown in black. This spectrum exhibits an onset of the TiO_2 conduction band at about +0.75 eV above the Fermi level (see Supporting Information). The LUMO peak positions of the N3 molecules vary substantially from 1.6 to 2 V. Note that for some molecules no STS peak was observed in the bias window in Figure 5b, in which STS measurements and tip conditions are stable. These spectra exemplify a series of STS data acquired on tens of N3 molecules that exhibit a wide

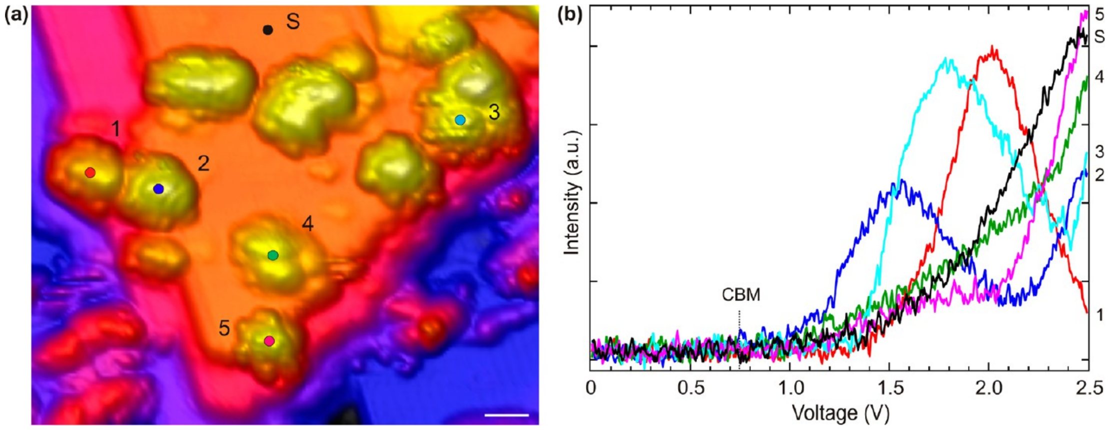

Figure 5. STS of individual N3 molecules on TiO_2 anatase (101). (a) STM overview image of various different N3 adsorption configurations (1.98 V, 0.08 nA, 5 K). (b) Corresponding dI/dV spectra taken at positions indicated in panel a (I = 0.08 nA, 5 K). The substrate conduction band minimum (CBM) was determined to +0.75 V. The N3 LUMO levels with respect to the substrate Fermi level vary strongly dependent on the specific N3 adsorption geometry. (Scale bar: (a) 2 nm.)

range of LUMO positions from 1.3 to 2.3 V. Hence, the data reveals a fundamental dependence of the N3 LUMO positions on the specific N3 binding mode to its environment. The width of the individual LUMO peaks amounts to about 400 mV. Previously performed molecular dynamics simulations identified a strong vibronic coupling of the occupied frontier N3 orbitals, introducing a thermal broadening of 180 meV.[42] Even at low temperature we expect a similarly strong broadening for the LUMO arising from the zero-point ionic motion. Furthermore since the LUMO and LUMO+1 energies are separated by less than 100 meV for N3 in the gas phase, this peak will consist of contributions from both states.

Across the range of STS spectra obtained here the N3 LUMO lies at least 0.5 eV above the conduction band edge, showing that fast electron injection should be possible for a range of binding geometries. On the other hand, adsorption geometries with high LUMO energies (such as spectrum 1 in Figure 5b) can be expected to suffer from reduced performance. The phonon-induced relaxation of the injected electron to the conduction band edge causes a "loss-in-potential", which is larger when the LUMO is higher in energy.[2] In order to minimize the loss-in-potential it is crucial to understand the atomistic mechanisms which determine the energy offset between conduction band edge and LUMO level. From calculations of the energy-level alignments for a set of candidate models of the N3/anatase interface (shown in Supporting Information Figure S5),[29,42] we found a substantial (0.88 eV) variation of the LUMO/conduction band edge offset across the adsorption geometries considered. This variation results from the interplay of several factors, namely the intrinsic electric dipole moment of the dye molecule,[4] the charge transfer at the interface,[42,43] and the screening of the photoexcited electron through image charge effects.[44] In addition to the above factors that have already been discussed in the literature, our calculations indicate that the energetics of the N3 LUMO can be sensitive to the distortion of the bipyridine units within the dye. Indeed, when N3 binds to the surface through two carboxylate anchor groups on the same BINA units, the strong Ti−O bonds induce an 11° tilt between the pyridine rings.[43] This tilt is responsible for a blueshift of the LUMO by 190 meV, as we checked by subjecting an isolated N3 molecule to the same distortion. These observations can be rationalized by noting that the N3 LUMO contains sizable contributions from the π^* manifold of the pyridines and that the strain disrupts the conjugation across the BINA unit.

Taken together our experimental observations and our calculations we provide new physical insights into the complexity of the N3/TiO_2 interface. The delicate interplay of several factors makes the identification of simple design rules for reducing the loss-in-potential challenging. Furthermore, even if one were able to minimize the loss-in-potential by engineering improved molecular chromophores, there would still remain the important questions of electron injection and recombination: a good dye needs to have its LUMO located near the substrate for efficient electron injection, and its highest occupied molecular orbital far from the substrate in order to prevent electron−hole recombination. This criterion has recently been implemented in a new class of push−pull dyes based on porphyrin derivatives.[45] Most importantly our work suggests that optimization strategies based solely on the electrochemical properties of the dye should be replaced by a more comprehensive approach where the focus is on the engineering of the chromophore−semiconductor interface at the atomic scale. This work shows unambiguously that in order to design more efficient photosensitizers it is crucial to consider kinetic aspects in the dye-substrate coupling, possible strain in the molecular chromophore, and the atomic-scale structure of the dye−semiconductor interface in such a way to achieve optimal photoelectron injection from all adsorbed photosensitizers.

Methods. Sample preparation and characterization were conducted in a UHV system (base pressure <2×10^{-10} mbar) equipped with a home-built low-temperature STM. The STM measurements were performed in constant current mode (bias voltage, 1.7− 2.0 V; tunnelling current, 0.06− 0.2 nA) at 5 K using electrochemically etched Pt−Ir tips. The dI/dV spectra were acquired using a lock-in amplifier modulating the bias voltage at a frequency of 2.5 kHz above the cutoff frequency of the feedback loop with an amplitude V_{rms} = 20 mV. Natural TiO_2 anatase single crystals with (101) surface orientation were prepared following reported protocols (see Supporting Information).[14,37] The cleaned substrates were transferred via a UHV suitcase to the soft landing, electrospray ion beam deposition (ES-IBD) source for the deposition of the nonvolatile N3 dye onto TiO_2 anatase (101) under UHV conditions at room temperature.[34] Intact, gas phase N3 ions are generated at ambient conditions by electrospray ionization (ESI)[46] of solutions of N3 dissolved in acetonitrile (analytical grade) at a concentration of 10^{-4} M. A home-built, highly efficient nanoelectrospray ionization source was used in negative ion mode at a spray voltage of −3500 V applied via a liquid junction to the electrospray emitter. Through a differentially pumped vacuum system of six stages, guided by radio frequency and dc-ion optics, the ions are conveyed to the sample in UHV. Time-of-flight mass spectrometry together with a quadrupole mass filter ensures the chemical purity of the beam (see Figure 1a). The ion beam was mass-selected to transmit only the singly charged N3 anion at 705 Th. A retarding grid energy detector is used to measure the kinetic energy of the beam. The kinetic energy was found in the range of 35−50 eV with a width of ±3 eV. The bias at the sample was set to +30 to +45 V, respectively, which lead to collision energies of (5 ± 3) eV. Under these conditions at the target in UHV, mass-selected currents of 60−150 pA are measured. The molecular coverage is controlled by online deposition current monitoring and integration. For a submonolayer coverage, a charge of 15 picoampere hours (pAh) is deposited. Subsequent to the N3 deposition, the sample was transferred to the STM using a home-built UHV transport suitcase. The intactness of the deposited N3 molecules was verified by SO_2-cluster induced desorption/ionization mass spectrometry experiments (see Figure 1b and Supporting Information). BINA molecules were deposited in situ at room temperature onto the substrate by organic molecular beam epitaxy from a quartz crucible heated to 522 K.

The theoretical modeling was performed within the generalized-gradient approximation to density functional theory.[47] The core−valence interaction was taken into account using ultrasoft pseudopotentials.[48] Periodic boundary conditions and plane-wave basis sets were used as implemented in the Quantum ESPRESSO package.[49] The electronic wave functions and densities were expanded up to kinetic energy cutoffs of 35 and 200 Ry, respectively. For the calculations on the isolated N3 dye, a simulation cell of dimensions $32 \times 32 \times 32$ Å^3 was used. The relaxed structure of the gas-phase molecule was obtained by minimizing the forces until the total force on each atom was less than 25 meV/Å. STM images of the dye were simulated in the Tersoff-Hamann approximation[50] with the local density-of-states (LDOS) integrated up to 0.2 eV above the N3 LUMO and plotted on a logarithmic scale.

For calculations of the BINA molecule on the TiO_2 surface, a twelve-layer anatase TiO_2 slab of dimensions 20.9×19.0 A^2 was used as in ref 29. Periodic images of the slab were separated by a vacuum region of 22 Å. A single BINA molecule was adsorbed on the slab and relaxed with the same 25 meV/A force criterion as for the isolated dye. The Tersoff-Hamann STM images were obtained by integrating the LDOS up to 1.2 eV above the anatase conduction band edge. This integration bound correctly captures the contribution from the LUMO of BINA, whose energy is calculated to be 1 eV above the conduction band edge. The map was calculated on a plane located 2 Å above the extremal BINA atom.

■ ASSOCIATED CONTENT

Supporting Information

Photograph and STM images of natural single crystal TiO_2 anatase (101) surface, dI/dV spectrum of pristine TiO_2 anatase (101), soft cluster-induced desorption/ionization mass spectrometry of N3, DFT adsorption geometries/energies of N3 dye adsorbed on TiO_2 anatase (101), interface models for N3 binding on TiO_2 anatase (101), manuscript Figure 5 at different substrate contrast, STM of N3 dye monolayer on TiO_2 anatase (101). This material is available free of charge via the Internet at http://pubs.acs.org.

■ AUTHOR INFORMATION

Corresponding Authors

*E-mail: c.kley@fkf.mpg.de.
*E-mail: sebastian.stepanow@mat.ethz.ch.

Notes

The authors declare no competing financial interest.

■ ACKNOWLEDGMENTS

We thank Professor Michael Grätzel for stimulating discussions. C.E.P. and F.G. acknowledge support from the European Research Council (EU FP7/ERC Grant 239578), the U.K. Engineering and Physical Sciences Research Council (Grant EP/J009857/1) and the Leverhulme Trust (Grant RL-2012-001). J.Č. acknowledges the support of Marie Curie Intra-European Fellowship of the 7th FP (AdaptNano, Project No. 251930) and CEITEC (CZ.1.05/1.1.00/02.0068).

■ ABBREVIATIONS

BINA, biisonicotinic acid; DFT, density functional theory; DSSC, dye-sensitized solar cell; ES-IBD, electrospray ion beam deposition; LDOS, local density-of-states; LUMO, lowest unoccupied molecular orbital; STM, scanning tunnelling microscopy; STS, scanning tunnelling spectroscopy

■ REFERENCES

(1) O'Regan, B.; Grätzel, M. *Nature* **1991**, *353*, 737−740.
(2) Hardin, B. E.; Snaith, H. J.; McGehee, M. D. *Nat. Photonics* **2012**, *6*, 162−169.
(3) Koops, S. E.; O'Regan, B. C.; Barnes, P. R. F.; Durrant, J. R. *J. Am. Chem. Soc.* **2009**, *131*, 4808−4818.
(4) De Angelis, F.; Fantacci, S.; Selloni, A.; Grätzel, M.; Nazeeruddin, M. K. *Nano Lett.* **2007**, *7*, 3189−3195.
(5) Murakoshi, K.; Kano, G.; Wada, Y .; Yanagida, S.; Miyazaki, H.; Matsumoto, M.; Murasawa, J. *J. Electroanal. Chem.* **1995**, *396*, 27−34.
(6) Mann, J. R.; Gannon, M. K.; Fitzgibbons, T. C.; Detty, M. R.; Watson, D. F. *J. Phys. Chem. C* **2008**, *112*, 13057−13061.
(7) Sasahara, A.; Fujio, K.; Koide, N.; Han, L.; Onishi, H. *Surf. Sci.* **2010**, *604*, 106−110.
(8) Wenger, B.; Grätzel, M.; Moser, J. E. *J. Am. Chem. Soc.* **2005**, *127*, 12150−12151.
(9) Zhang, S.; Yang, X.; Numata, Y.; Han, L. *Energy Environ. Sci.* **2013**, *6*, 1443−1464.
(10) Watson, D. F.; Meyer, G. J. *Annu. Rev. Phys. Chem.* **2005**, *56*, 119−156.
(11) Pellnor, M.; Myllyperkiö, P.; Korppi-Tommola, J.; Yartsev, A.; Sundström, V. *Chem. Phys. Lett.* **2008**, *462*, 205−208.
(12) Teuscher, J.; Decoppet, J. D.; Punzi, A.; Zakeeruddin, S. M.; Moser, J. E.; Grätzel, M. *J. Phys. Chem. Lett.* **2012**, *3*, 3786−3790.
(13) Barbé, C. J.; Arendse, F.; Comte, P.; Jirousek, M.; Lenzmann, F.; Shklover, V.; Grätzel, M. *J. Am. Ceram. Soc.* **1997**, *12*, 3157−3171.
(14) Hebenstreit, W.; Ruzycki, N.; Herman, G. S.; Gao, Y.; Diebold, U. *Phys. Rev. B* **2000**, *62*, 16334.
(15) Nazeeruddin, M. K.; Kay, A.; Rodicio, I.; Humphry-Baker, R.; Mueller, E.; Liska, P.; Vlachopoulos, N.; Graetzel, M. *J. Am. Chem. Soc.* **1993**, *115*, 6382−6390.
(16) Hagfeldt, A.; Grätzel, M. *Acc. Chem. Res.* **2000**, *33*, 269−277.
(17) Nazeeruddin, M. K.; Zakeeruddin, S. M.; Humphry-Baker, R.; Jirousek, M.; Liska, P.; Vlachopoulos, N.; Shklover, V.; Fischer, C. H.; Grätzel, M. *Inorg. Chem.* **1999**, *38*, 6298−6305.

(18) Nazeeruddin, M. K.; Pechy, P.; Renouard, T.; Zakeeruddin, S. M.; Humphry-Baker, R.; Comte, P.; Liska, P.; Cevey, L.; Costa, E.; Shklover, V.; Spiccia, L.; Deacon, G. B.; Bignozzi, C. A.; Graetzel, M. *J. Am. Chem. Soc.* **2001**, *123*, 1613−1624.

(19) Sasahara, A.; Pang, C. L.; Onishi, H. *J. Phys. Chem. B* **2006**, *110*, 4751−4755.

(20) Mayor, L. C.; Ben Taylor, J.; Magnano, G.; Rienzo, A.; Satterley, C. J.; O'Shea, J. N.; Schnadt, J. *J. Chem. Phys.* **2008**, *129*, 114701.

(21) Hugot-Le Goff, A.; Falaras, P. *J. Electrochem. Soc.* **1995**, *142*, 38−41.

(22) Falaras, P.; Grätzel, M.; Hugot-Le Goff, A.; Nazeeruddin, M.; Vrachnou, E. *Electrochem. Soc. Lett.* **1993**, *140*, 92−94.

(23) Haukka, M.; Hirva, P. *Surf. Sci.* **2002**, *511*, 373−378.

(24) Deacon, G. B.; Phillips, R. J. *Coord. Chem. Rev.* **1980**, *33*, 227.

(25) Finnie, K. S.; Bartlett, J. R.; Woolfrey, J. L. *Langmuir* **1998**, *14*, 2744−2749.

(26) Nazeeruddin, M. K.; Humphry-Baker, R.; Liska, P.; Grätzel, M. *J. Phys. Chem. B* **2003**, *107*, 8981−8987.

(27) Rensmo, H.; Westermark, K.; Sodergren, S.; Kohle, O.; Persson, P.; Lunell, S.; Siegbahn, H. *J. Chem. Phys.* **1999**, *111*, 2744−2750.

(28) Schiffmann, F.; VandeVondele, J.; Hutter, J.; Wirz, R.; Urakawa, A.; Baiker, A. *J. Phys. Chem. C* **2010**, *114*, 8398−8404.

(29) Patrick, C. E.; Giustino, F. *Phys. Rev. B* **2011**, *84*, 085330.

(30) De Angelis, F.; Fantacci, S.; Selloni, A.; Nazeeruddin, M. K.; Grätzel, M. *J. Phys. Chem. C* **2010**, *114*, 6054−6061.

(31) Zuleta, M.; Edvinsson, T.; Yu, S.; Ahmadi, S.; Boschloo, G.; Gothelid, M.; Hagfeldt, A. *Phys. Chem. Chem. Phys.* **2012**, *14*, 10780−10788.

(32) Pastore, M.; De Angelis, F. *J. Phys. Chem. Lett.* **2013**, *4*, 956−974.

(33) Hara, K.; Sato, T.; Katoh, R.; Furube, A.; Ohga, Y.; Shinpo, A.; Suga, S.; Sayama, K.; Sugihara, H.; Arakawa, H. *J. Phys. Chem. B* **2003**, *107*, 597−606.

(34) Rauschenbach, S.; Vogelgesang, R.; Malinowski, N.; Gerlach, J. W.; Benyoucef, M.; Costantini, G.; Deng, Z.; Thontasen, N.; Kern, K. *ACS Nano* **2009**, *3*, 2901−2910.

(35) Kahle, S.; Deng, Z.; Malinowski, N.; Tonnoir, C.; Forment-Aliaga, A.; Thontasen, N.; Rinke, G.; Le, D.; Turkowski, V.; Rahman, T. S.; Rauschenbach, S.; Ternes, M.; Kern, K. *Nano Lett.* **2012**, *12*, 518−521.

(36) Gebhardt, C. R.; Tomsic, A.; Schröder, H.; Dürr, M.; Kompa, K. L. *Angew. Chem., Int. Ed.* **2009**, *48*, 4162−4165.

(37) Gong, X.-Q.; Selloni, A.; Batzill, M.; Diebold, U. *Nat. Mater.* **2006**, *5*, 665−670.

(38) Schnadt, J.; Bruhwiler, P. A.; Patthey, L.; O'Shea, J. N.; Sodergren, S.; Odelius, M.; Ahuja, R.; Karis, O.; Bassler, M.; Persson, P.; Siegbahn, H.; Lunell, S.; Martensson, N. *Nature* **2002**, *418*, 620−623.

(39) Labat, F.; Adamo, C. *J. Phys. Chem. C* **2007**, *111*, 15034−15042.

(40) Schnadt, J.; Henningsson, A.; Andersson, M. P.; Karlsson, P. G.; Uvdal, P.; Siegbahn, H.; Bruhwiler, P. A.; Sandell, A. *J. Phys. Chem. B* **2004**, *108*, 3114−3122.

(41) Hirva, P.; Haukka, M. *Langmuir* **2010**, *26*, 17075−17081.

(42) Patrick, C. E.; Giustino, F. *Phys. Rev. Lett.* **2012**, *109*, 116801.

(43) Labat, F.; Ciofini, I.; Hratchian, H. P.; Frisch, M. J.; Raghavachari, K.; Adamo, C. *J. Phys. Chem. C* **2011**, *115*, 4297−4306.

(44) Neaton, J. B.; Hybertsen, M. S.; Louie, S. G. *Phys. Rev. Lett.* **2006**, *97*, 216405.

(45) Yella, A.; Lee, H. W.; Tsao, H. N.; Yi, C. Y.; Chandiran, A. K.; Nazeeruddin, M. K.; Diau, E. W. G.; Yeh, C. Y.; Zakeeruddin, S. M.; Grätzel, M. *Science* **2011**, *334*, 629−634.

(46) Fenn, J. B.; Mann, M.; Meng, C. K.; Wong, S. F.; Whitehouse, C. M. *Science* **1989**, *246*, 64−71.

(47) Perdew, J. P.; Burke, K.; Ernzerhof, M. *Phys. Rev. Lett.* **1996**, *77*, 3865−3868.

(48) Vanderbilt, D. *Phys. Rev. B* **1990**, *41*, 7892−7895.

(49) Giannozzi, P.; Baroni, S.; Bonini, N.; Calandra, M.; Car, R.; Cavazzoni, C.; Ceresoli, D.; Chiarotti, G. L.; Cococcioni, M.; Dabo, I.; Corso, A. D.; de Gironcoli, S.; Fabris, S.; Fratesi, G.; Gebauer, R.; Gerstmann, U.; Gougoussis, C.; Kokalj, A.; Lazzeri, M.; Martin-Samos, L.; Marzari, N.; Mauri, F.; Mazzarello, R.; Paolini, S.; Pasquarello, A.; Paulatto, L.; Sbraccia, C.; Scandolo, S.; Sclauzero, G.; Seitsonen, A. P.; Smogunov, A.; Umari, P.; Wentzcovitch, R. M. *J. Phys.: Condens. Matter* **2009**, *21*, 395502.

(50) Tersoff, J.; Hamann, D. R. *Phys. Rev. B* **1985**, *31*, 805−813.